

Truncated mass divergence in a Mott metal

Konstantin Semeniuk,^{1,†} Hui Chang,¹ Jordan Baglo,^{1,‡} Sven Friedemann,² Audrey Grockowiak,^{3,§} William A. Coniglio,³ Monika Gamza,⁴ Pascal Reiss,^{1,5,||} Patricia Alireza,¹ Inge Leermakers,⁶ Alix McCollam,⁶ Stan Tozer,³ and F. Malte Grosche^{1,*}

¹*Cavendish Laboratory, University of Cambridge, Cambridge CB3 0HE, United Kingdom*

²*H H Wills Laboratory, University of Bristol, Bristol BS8 1TL, United Kingdom*

³*National High Magnetic Field Laboratory, Tallahassee, FL 83810, USA*

⁴*Jeremiah Horrocks Institute for Mathematics, Physics and Astronomy, University of Central Lancashire, Preston PR1 2HE, UK*

⁵*Clarendon Laboratory, University of Oxford, Oxford OX1 3PU, United Kingdom*

⁶*High Field Magnet Laboratory (HFML-EMFL), Radboud University, Toernooiveld 7, 6525 ED Nijmegen, The Netherlands*

(Dated: February 9, 2022)

Metal-insulator transitions in clean, crystalline solids can be driven by two distinct mechanisms. In a conventional insulator, the charge carrier concentration vanishes, when an energy gap separates filled and unfilled electronic states. In the established picture of a Mott insulator [1], by contrast, electronic interactions cause coherent charge carriers to slow down and eventually stop in electronic gridlock without materially affecting the carrier concentration itself. This description has so far escaped experimental verification by quantum oscillation measurements, which directly probe the velocity distribution of the coherent charge carriers. By extending this technique to high pressure we were able to examine the evolution of carrier concentration and velocity in the strongly correlated metallic state of the clean, crystalline material NiS₂, while tuning the system towards the Mott insulating phase. Our results confirm that pronounced electronic slowing down indeed governs the approach to the insulating state. However, the critical point itself, at which the carrier velocity would reach zero and the effective carrier mass diverge, is concealed by the insulating sector of the phase diagram. In the resulting, more nuanced view of Mott localisation, the inaccessibility of the low temperature Mott critical point resembles that of the threshold of magnetic order in clean metallic systems, where criticality is almost universally interrupted by first order transitions [2], tri-

critical behaviour [3] or novel emergent phases such as unconventional superconductivity [4].

Mott localisation is one of the most fundamental consequences of electronic interactions in solids [5]. Its theoretical understanding feeds into numerous related research areas, ranging from cuprate superconductivity to Kondo lattice materials and correlated topological insulators [6, 7]. The Mott insulating state [8] is stabilised near half-filling, when the on-site repulsion energy U exceeds a threshold value U_c . In the simplest case laid out in the Hubbard model [9], this threshold is determined by the kinetic energy contribution to the total energy. Various factors further affect U_c , for instance charge transfer into additional bands near the Fermi energy or more than one half-filled state per lattice site and the resulting Hund's rule coupling. Although quantum materials of current interest often require more elaborate models that reflect, for instance, the interplay of slow and fast carriers in Kondo lattice systems, key aspects of these materials connect back to the Hubbard model, such as the notion of orbitally selective Mott transitions in multiband systems [10–13].

In the canonical description formulated by Brinkman and Rice [1], Mott localisation is driven not by reduction of charge carrier concentration (as is the case in band insulators) but rather by a gradual slowing down of the charge carriers, while the volume enclosed by the Fermi surface remains constant in line with Luttinger's theorem [14]. In this description, the reduction of the Fermi velocity of strongly correlated Landau quasiparticles is reflected in a reduction of the quasiparticle weight z towards zero and a concomitant rise and, ultimately, divergence of the quasiparticle effective mass m^* . More sophisticated calculations within dynamic mean field theory (DMFT) have supported this scenario for the evolution of the correlated metallic state in the low temperature limit for a purely electronic Mott transition [15–19]. As illustrated in Figure 1, these calculations indicate that the transition is first order at finite temperature, that it is accompanied by a range in which metallic and insulating states can coexist (dotted region in Figure 1) and that the

K.S., H.C., and J.B. contributed equally to this work

[†] Now at Max Planck Institute for Chemical Physics of Solids, Dresden 01187, Germany

[‡] Now at Department of Physics, Université de Sherbrooke, Sherbrooke J1K 2R1, Canada

[§] Now at Brazilian Synchrotron Light Laboratory, Brazilian Center for Research in Energy and Materials, 13083-970 Campinas, São Paulo, Brazil

^{||} Now at Max Planck Institute for Solid State Research, Stuttgart 70569, Germany

* Corresponding Author: fmg12@cam.ac.uk

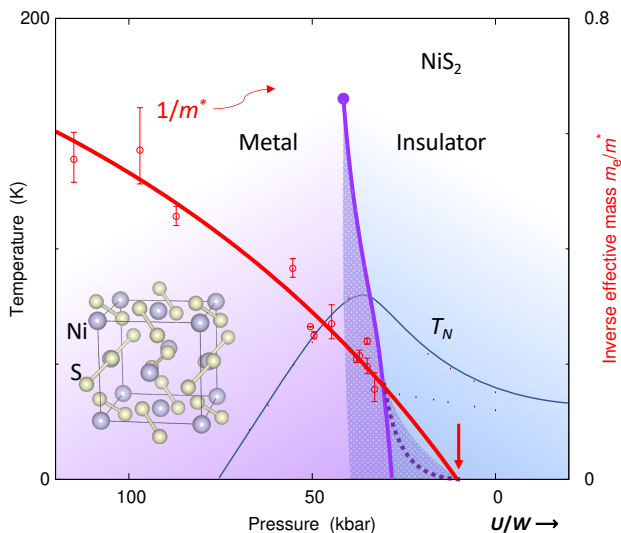


Figure 1. Mott metal insulator transition in NiS_2 , which is metallic at high pressure (large effective bandwidth W and therefore small ratio U/W) and insulating at low pressure. Magnetic order sets in below a transition temperature T_N (blue line, following experimental data [20, 21]). The Mott transition line (purple, from resistivity data [22]) ends in a critical point at high temperature. Its first-order nature implies the possibility of metastable states (dotted region) surrounding the thermodynamic transition line. At low temperature, the transition line in DMFT calculations curves away towards higher U/W (dashed purple line), ending in a zero-temperature critical point [17–19] (thick red arrow). The inverse carrier mass extracted in this study (red circles with errorbars) extrapolates to zero deep inside the region of the phase diagram where transport measurements show insulating behaviour.

transition line bends sharply as the zero temperature limit is approached (dashed line in Figure 1).

Given the central importance of Mott physics for understanding quantum materials it may be surprising that experimental tests of the Brinkman-Rice paradigm are comparatively scarce. Spectroscopic measurements such as photoemission spectroscopy (PES) [23, 24] examine the suppression of the quasiparticle weight in the strongly correlated metal near Mott localisation, and they can track the spectrum close to and well away from the Fermi energy [25]. However, the limited energy resolution of PES and its inability to distinguish between the coherent and incoherent parts of the spectrum hinder high precision measurements of the coherent low-energy excitations that constitute long-lived Landau quasiparticles, as is apparent for instance in [26]. PES also tends to be limited to elevated temperatures, and it cannot be undertaken under pressure, which presents a clean way to tune in small steps across a Mott transition without doping-induced disorder.

Conversely, the Landau quasiparticles at the core of the Brinkman-Rice picture are detected directly by observing quantum oscillatory phenomena in high magnetic fields. These probe the quasiparticle spectrum, making it possible to track the quasiparticle

mass and Fermi surface as Mott localisation is approached with superior resolution. Quantum oscillation measurements have already contributed to reports of a divergent form of the quasiparticle mass at the *magnetic* quantum critical points in CeRhIn_5 and $\text{BaFe}_2(\text{As}_{1-x}\text{P}_x)_2$ [27, 28].

Here, we study the clean Mott insulator NiS_2 and use high-pressure quantum oscillation measurements as a direct probe of the coherent quasiparticles and their Fermi velocity. Our data confirm key tenets of the Brinkman-Rice picture, namely that charge carrier concentration is conserved but carrier mass takes on a divergent form on approaching Mott localisation. In contrast to the Brinkman-Rice picture, however, we find that the carrier mass divergence extrapolates to a critical point buried well inside the insulating state.

The cubic sulphide NiS_2 offers an excellent opportunity to investigate the correlated Mott metal, because high purity single crystals are available [21, 29] and a moderate pressure of about 30 kbar is sufficient to reach the metallic state [21, 22, 30, 31] (Figure 1). A previous study demonstrated that quantum oscillations can be observed under these conditions [22]. Avoiding doping and the associated disorder, this affords a direct view on the evolution of quasiparticle properties within the correlated metallic state.

The detection of quantum oscillations under pressure in NiS_2 [22] builds on three innovations : (i) Te-flux growth [29] reliably produces high quality crystals matching the best vapour-transport grown NiS_2 reported previously [21], with residual resistivities of $\simeq 1 \mu\Omega\text{cm}$ at high pressure [22]; (ii) tank circuit radio frequency tunnel diode oscillator (TDO) techniques [32, 33] with a microcoil placed inside the $< 400 \mu\text{m}$ diameter high pressure sample space enable ultra-sensitive, contact-free measurements of skin depth or magnetic susceptibility oscillations in applied field at high pressures (Figure 2d); (iii) miniature anvil cells and novel gasket preparation techniques allow access to the 100 kbar range and beyond in narrow-bore dilution refrigerator probes or on rotator stages while preserving excellent pressure homogeneity [34]. Combined with superheterodyne signal detection [35], such a setup can resolve quantum oscillations at the level of 0.01 ppm.

High-pressure quantum oscillations

The Fermi surface signatures detected in our quantum oscillation measurements in NiS_2 closely match density functional theory (DFT) calculations for the largest Fermi surface sheet [35]. We observe strong quantum oscillations with a frequency $F \simeq 6.17 \text{ kT}$ as illustrated in (Figure 2) at a pressure of 50 kbar, well above the metallisation pressure of 30 kbar. This frequency is in close agreement with our earlier measurements at 38 kbar and with the accompanying DFT calculations [22]. It corresponds to a cross-sectional area $A_k = 0.589 \text{ \AA}^{-2}$ for $B||c$, nearly half the cross-sectional area of the first Brillouin zone (BZ) $A_{BZ} = 1.27 \text{ \AA}^{-2}$. The angular dependence of the quantum oscillation frequency closely matches expectations from

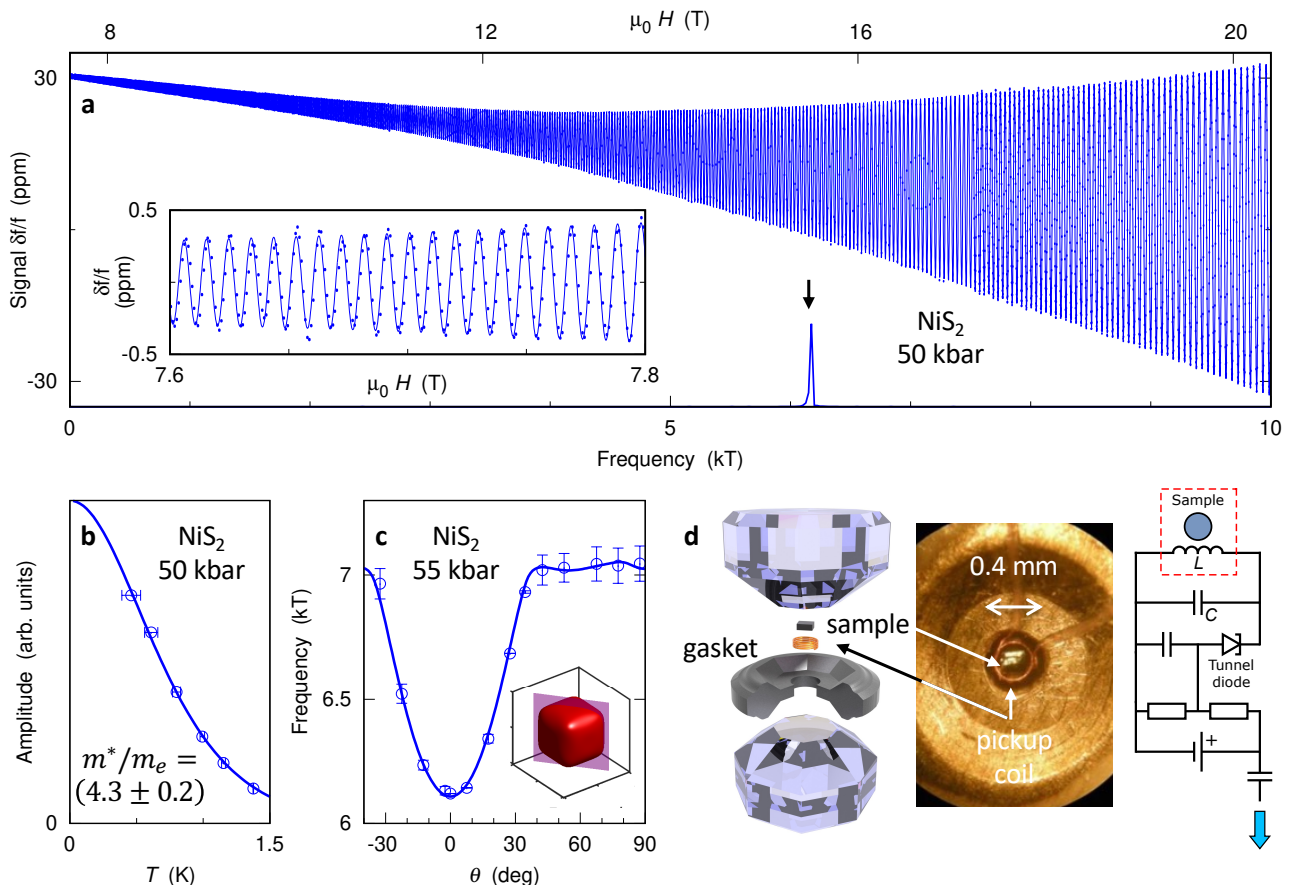


Figure 2. Quantum oscillations in NiS₂. **a**, Quantum oscillations are clearly resolved well above the metallisation pressure, down to fields as low as < 8 T (inset). The power spectrum shows a single peak at 6.17 kT (lower axis). **b,c**, The QO amplitude (**b**) follows the Lifshitz-Kosevich form as a function of temperature (solid line), with effective mass $m^* \simeq 4.3 m_e$, and a rotation study (**c**) at a nearby pressure produces an angle dependence of the QO frequency that closely matches expectations (solid line) for a cube-shaped FS pocket (inset). **d**, Key elements of the experimental setup.

a cube-shaped Fermi surface pocket (Figure 2c). A hole pocket of almost identical size and shape is the dominant feature in *ab initio* DFT calculations within the paramagnetic metallic state [22], confirming the assignment of these quantum oscillations to the cube-shaped hole surface. A small splitting of the quantum oscillation frequency at lower pressures (top panel in Figure 3a) can be attributed to the effect of magnetic ordering [35]. Whereas *ab initio* DFT calculations can accurately reflect the Fermi surface geometry, they capture electronic correlations insufficiently to produce reliable estimates of the true carrier mass, which can be detected directly in quantum oscillation measurements.

The carrier mass is strongly renormalised. The effective quasiparticle mass $m^* = 4.3m_e$ (m_e - free electron mass) determined at 50 kbar from the temperature dependence of the oscillation amplitude (Figure 2b) exceeds the *ab initio* band mass $m_b = 0.8m_e$ obtained for this hole pocket by a factor of 5.4, indicating substantial mass renormalisation comparable to the highest values observed by quantum oscillation measurements in any transition metal compound [36, 37]. This highlights the strongly correlated nature of the metallic state in NiS₂.

The Fermi surface volume is preserved over the

full pressure range, indicating that the charge carrier concentration remains constant on approaching the metal-insulator transition. The pressure dependence of the quantum oscillation frequency and carrier mass, based on 14 high pressure runs reaching up to ~ 115 kbar, are summarised in Figure 3. The pressure dependence of the quantum oscillation frequency can be attributed to the compressibility of NiS₂ as indicated by the solid line in Figure 3b. We use the change of unit cell volume determined from X-ray diffraction to estimate the effect of pressure on the Fermi-surface volume [35]. Transport measurements in the Ni(S/Se)₂ composition series indicate increases in resistivity and Hall coefficient on approaching the insulating threshold by reducing the Se content, which could be interpreted in terms of a decreasing carrier concentration [39]. Our data show that this scenario does not apply in pressure-metallised NiS₂: the nearly constant quantum oscillation frequencies observed right up to the insulating state demonstrate that no significant change in the carrier concentration is taking place. We note that quantum oscillations directly probe the Fermi surface volume in reciprocal space, whereas contrary inferences from Hall effect measurements [39] may suffer from the effects of inhomogeneities and magnetic contributions.

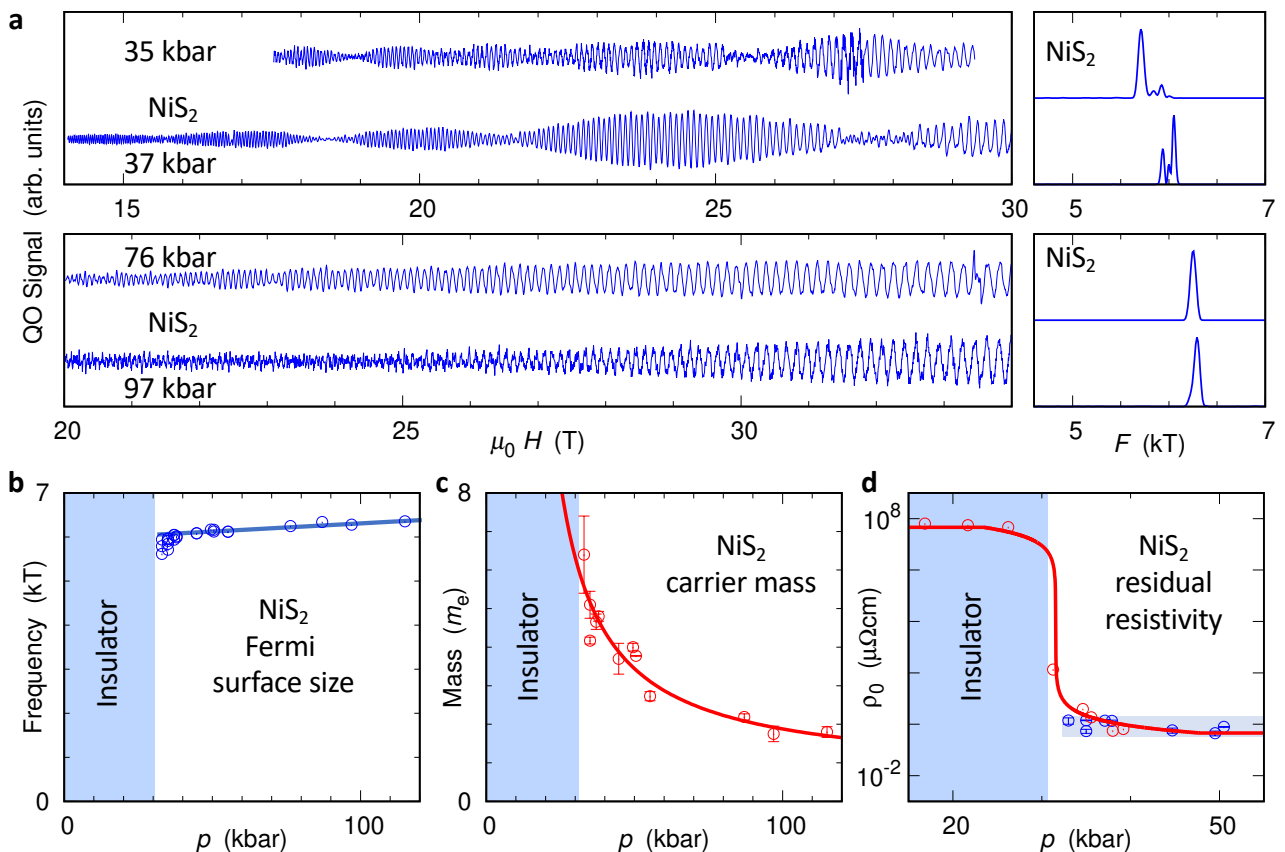


Figure 3. Pressure evolution of the electronic structure of NiS₂. **a**, Quantum oscillations in NiS₂ at selected pressures (scaled and off-set for clarity), with corresponding power spectra to the right. **b-d**, Pressure dependences of the quantum oscillation frequency (**b**), the effective quasiparticle mass (**c**) and the residual resistivity ρ_0 (**d**). The blue line in panel **b** is a linear least-squares fit to the frequency coming from the cubic Fermi surface (highest frequency at each pressure). The red line in panel **c** is a least-squares fit consistent with the one shown in Figure 1 (see text). Whereas the effective mass is enhanced by about a factor of three over the investigated pressure range on approaching Mott localisation, the frequency and thereby the Fermi surface cross-section changes only slightly, at a rate which is broadly consistent with the change of the unit cell volume. Panel **d** compares ρ_0 determined in high pressure transport measurements [22] (red markers), to ρ_0 expected from the electronic mean free paths determined from the quantum oscillation analysis (blue markers). Whereas the quantum-oscillation-derived mean free path and the resulting ρ_0 are pressure independent (blue shaded region), direct transport measurements show a strong increase of ρ_0 on approaching the metal-insulator threshold from high pressures. This discrepancy suggests a significant and increasing volume fraction of insulating regions close to the metal-insulator threshold, which we model within 3D effective medium theory (red line). We ascribe the saturation of the transport-derived ρ_0 below 30 kbar to surface conduction [38].

The carrier mass is strongly boosted on approaching the Mott metal-insulator transition, suggesting critical slowing down of the coherent quasiparticles. We observe a monotonic 3-fold increase of the quantum oscillation mass between 120 kbar and $\simeq 30$ kbar (Figure 3c). This rules out magnetic quantum criticality associated with the threshold of antiferromagnetism at ≈ 80 kbar [40] as the primary driver of the mass enhancement. The effective mass of the coherent quasiparticles in NiS₂ is enhanced up to seven-fold above the bare (DFT) band mass, which in our calculations shows negligible pressure dependence over the range investigated experimentally.

While the carrier mass follows a divergent form consistent with the Brinkman-Rice scenario over a wide range of pressure, the critical point for the mass divergence is buried within the insulating part of the phase diagram. The quasiparticle mass is expected to diverge as $1/(p - p_c)$ within the Brinkman-Rice

picture close to a critical pressure p_c . More generally, the inverse mass enhancement given in [1] follows $m_e/m^* = 1 - (U/U_0)^2$, where U_0 is proportional to the band width and can be expanded to first order in pressure p : $U_0 = A(p + a)$, with constant coefficients A and a . At the critical pressure p_c , $U_0 = A(p_c + a) = U$, leading to the simpler expression for the inverse mass renormalisation $m_e/m^* = 1 - ((p_c + a)/(p + a))^2$. This expression closely fits the pressure dependence of the quantum oscillation mass (Figure 3c), with a critical pressure $p_c \simeq 10(1)$ kbar well below the metallisation pressure of about 30 kbar determined from transport experiments [22]. The inverse mass enhancement, likewise, is shown in Figure 1 to extrapolate to zero inside the insulating regime.

The resulting phase diagram (Figure 1) is consistent with DMFT studies for a purely electronic Mott transition [15–19]. As mentioned in the introduction, the first-order thermodynamic transition line in

these calculations bends sharply towards higher coupling at low T , and it is surrounded by a region in which both metallic and insulating states coexist, one being thermodynamically stable, the other metastable. Below the pressure of the high T critical point, $p_h \simeq 44$ kbar, the low temperature state is accessed by cooling through the transition line which overhangs the metallic region of the phase diagram. If the thermodynamic transition line is crossed at sufficiently high temperature, enough of the material converts into the metallic state to enable the observation of quantum oscillations. The reduction in QO signal amplitude and the rise in ρ_0 on approaching the metal-insulator transition in NiS₂ [22] (Figure 3d) as well as Ni(S/Se)₂ [39] suggest that the metallic volume fraction is already strongly reduced well before the metal insulator transition itself is reached. In this purely electronically driven scenario, the metallic volume fraction diminishes as the second-order low temperature end point of the Mott transition is approached, truncating the observed mass divergence. Coupling to the lattice, which causes a discontinuous volume change, can further exacerbate the first-order nature of the MIT and extend it to zero temperature [41], folding away the section of the pressure-temperature phase diagram surrounding the second-order low temperature end point of the transition line, which thereby becomes inaccessible to experiment.

This interpretation is consistent with high pressure x-ray data, which reported evidence for phase coexistence near metallisation in NiS₂ [42], with ARPES data in Ni(S/Se)₂, which indicates that the Fermi velocity v_F extrapolates to zero within the insulating part of the phase diagram [25, 26], and with high pressure heat capacity measurements in V₂O₃, in which the divergence of the Sommerfeld coefficient does not occur at the metal insulator transition but rather can be extrapolated well into the insulating phase [43].

In summary, our high pressure quantum oscillation measurements allow the first comprehensive survey of the electronic structure and its evolution on the metallic side of a pressure-induced Mott insulator transition in ultra-clean specimens with a simple crystal structure. A large Fermi surface pocket is detected in pressure-metallised NiS₂, which corresponds closely to expectations from band structure calculations. On approaching Mott localisation from the metallic side, the Fermi surface volume remains comparatively unaffected right up until metallic behaviour is lost. The carrier mass, on the other hand, rises in a clean, divergent form with unprecedented dynamic range for correlation-induced mass renormalisation.

Our results complement the central tenets of the Brinkman-Rice picture with the realisation that in this cubic system the expected mass divergence on approaching Mott localisation is truncated by the consequences of a first order phase transition, reminiscent of the fate of *magnetic* quantum critical points in metallic magnets [2]. Resolving the precise origin of this phenomenon may be a challenge for future experiments which could, for instance, approach the

critical pressure from the metallic side at low temperature in a variable-pressure device. Our results furthermore demonstrate the power of anvil cell based quantum oscillation measurements extending into the > 100 kbar regime for addressing challenging questions in fundamental condensed matter research. This provides a powerful complement to ARPES studies, which are limited to ambient conditions, and opens up a wide range of long-standing problems for closer investigation. The metallic state on the threshold of a Mott insulator transition is a central research theme in modern condensed matter physics. Its relevance is born out by the intense effort devoted to the normal state of the high temperature superconducting cuprates. Additional complexity arises from coupling to the lattice [41, 44], orbital degeneracy and Hund's rule coupling [25, 45, 46], phase separation and percolation [47], colossal susceptibility to applied electric field or strain [48–50] and novel electronic surface or bulk states [51]. The methodology developed for this study may help investigate these and other challenging phenomena that arise in the correlated metallic state on the threshold of Mott localisation – or more generally near pressure-induced quantum phase transitions.

METHODS

Synthesis of NiS₂ single crystals. Single-crystal samples were grown with the tellurium-flux method as described earlier [29]. Ultra-low sulphur deficiency was determined from X-ray diffraction results as detailed in [22].

Tunnel-diode-oscillator measurements at high pressures. Quantum oscillations were measured via a contactless skin-depth probing technique based on the tunnel diode oscillator (TDO)—an inductor-capacitor oscillator sustained by a tunnel diode [32]. The inductors in our experiments were 3-10 turn cylindrical coils with inner diameters of 80 μm – 200 μm wound with 12 μm – 15 μm insulated copper wires. The coils were mounted inside the < 400 μm diameter sample spaces of BeCu or composite [34] gaskets of diamond/moissanite anvil cells. Samples of NiS₂ were obtained by cleaving oriented single crystals into rectangular cuboids of 10 μm – 100 μm thickness and 50 μm – 120 μm length and width, and were placed inside the coils. Our setup monitored the resonance frequency of the TDO. Changes in resistivity or magnetic susceptibility of NiS₂ in the metallic state were detected as proportional shift in the resonance frequency, due to a change in the flux expulsion caused by the skin effect, which depends on resistivity and magnetic susceptibility [35]. Wirings of the cryostats were optimised to allow the oscillator to operate at frequencies of up to 500 MHz [35]. To ensure good hydrostaticity we used the 4:1 methanol-ethanol mix or 7474 Daphne oil (only at 55 kbar) as pressure-transmitting media. Pressure was deter-

mined via ruby fluorescence spectroscopy at low temperature. Quantum oscillations measurements were carried out at the NHMFL, Tallahassee, and at the HFML, Nijmegen, in top-loading ^3He and dilution refrigeration cryostats with magnetic field strengths of up to 35 T, and at the superconducting high field facility in the Cavendish Laboratory, Cambridge, using a dilution refrigerator insert and fields of up to 18.4 T.

Analysis of quantum oscillations. The cross-sectional area A_k associated with a cyclotron orbit in strong magnetic fields is determined via the Onsager formula [52] $A_k = \frac{2\pi e}{\hbar} F$, where e and \hbar are the elementary charge and Planck's constant, respectively. The quasiparticle mass and the mean free path were obtained via the full Lifshitz-Kosevich formula fitting [35]. The quasiparticle mass m^* was additionally extracted by fitting the temperature (T) dependence of the quantum oscillation amplitude \tilde{y} at a fixed magnetic field B with the Lifshitz-Kosevich expression $\tilde{y} = \alpha T \left[\sinh \left(14.639 \text{ TK}^{-1} \frac{T}{B} \frac{m^*}{m_e} \right) \right]^{-1}$, where α is a temperature-independent factor and m_e is the bare electron mass.

ADDITIONAL INFORMATION

Acknowledgements. We thank, in particular, A. Chubukov, G. Lonzarich, and M. Sutherland for helpful discussions. The work was supported by the EPSRC of the UK (grants no. EP/K012894 and EP/P023290/1), and by Trinity College. Portions of this work were performed at the National High Magnetic Field Laboratory, which is supported by the National Science Foundation Cooperative Agreement No. DMR-1157490 and DMR-1644779 and the State of Florida, and at HFML-RU/NWO-I a part of the European Magnetic Field Laboratory (EMFL), which is supported by the EPSRC of the UK via its membership to the EMFL (grant no. EP/N01085X/1).

Author contributions. K.S., H.C., and J.B. contributed equally to this work. S.F. and F.M.G. conceived the experiment. S.F. and M.G. grew and characterised the NiS_2 single crystals. H.C. designed the TDO setup. H.C., A.G., and P.A. closed the high-pressure anvil cells. K.S., J.B., H.C., S.F., P.R., and F.M.G. conducted the quantum oscillation measurements. A.G., W.A.C., and S.T. provided technical support at NHFML Tallahassee. I.L. and A.M. provided technical support at HFML Nijmegen. K.S., J.B., H.C., S.F., P.R., and F.M.G. analysed the experimental data. P.R. performed the band structure and effective medium theory calculations. K.S., S.F., P.R., and F.M.G. co-wrote the manuscript.

Competing Interests. The authors declare no competing interests.

Correspondence and requests for materials should be addressed to F. Malte Grosche (fmg12@cam.ac.uk).

-
- [1] W. F. Brinkman and T. M. Rice. Application of Gutzwiller's Variational Method to the Metal-Insulator Transition. *Phys. Rev. B*, 2(10):4302–4304, November 1970. URL <https://doi.org/10.1103/PhysRevB.2.4302>.
 - [2] M. Brando, D. Belitz, F. M. Grosche, and T. R. Kirkpatrick. Metallic quantum ferromagnets. *Rev. Mod. Phys.*, 88(2):025006, May 2016. URL <https://doi.org/10.1103/RevModPhys.88.025006>.
 - [3] Sven Friedemann, Will J. Duncan, Max Hirschberger, Thomas W. Bauer, Robert Küchler, Andreas Neubauer, Manuel Brando, Christian Pfeleiderer, and F. Malte Grosche. Quantum tricritical points in NbFe_2 . *Nature Phys*, 14(1):62–67, January 2018. URL <https://doi.org/10.1038/nphys4242>.
 - [4] N. D. Mathur, F. M. Grosche, S. R. Julian, I. R. Walker, D. M. Freye, R. K. W. Haselwimmer, and G. G. Lonzarich. Magnetically mediated superconductivity in heavy fermion compounds. *Nature*, 394(6688):39–43, July 1998. URL <https://doi.org/10.1038/27838>.
 - [5] Masatoshi Imada, Atsushi Fujimori, and Yoshinori Tokura. Metal-insulator transitions. *Rev. Mod. Phys.*, 70(4):225, 1998. URL <https://doi.org/10.1103/RevModPhys.70.1039>.
 - [6] Patrick A. Lee, Naoto Nagaosa, and Xiao-Gang Wen. Doping a Mott insulator: Physics of high-temperature superconductivity. *Rev. Mod. Phys.*, 78(1):17–85, January 2006. URL <https://doi.org/10.1103/RevModPhys.78.17>.
 - [7] Maxim Dzero, Jing Xia, Victor Galitski, and Piers Coleman. Topological Kondo Insulators. *Annu. Rev. Condens. Matter Phys.*, 7(1):249–280, March 2016. URL <http://doi.org/10.1146/annurev-conmatphys-031214-014749>.
 - [8] Neville F. Mott. The Basis of the Electron Theory of Metals, with Special Reference to the Transition Metals. *Proc. Phys. Soc. Sect. A*, 62(7):416–422, July 1949. URL <http://doi.org/10.1088/0370-1298/62/7/303>.
 - [9] John Hubbard. Electron correlations in narrow energy bands. *Proc. R. Soc. Lond. A*, 276(1365):238–257, 1963. URL <https://doi.org/10.1098/rspa.1963.0204>.
 - [10] Matthias Vojta. Orbital-Selective Mott Transitions: Heavy Fermions and Beyond. *J. Low Temp. Phys.*, 161(1-2):203–232, October 2010. URL <http://doi.org/10.1007/s10909-010-0206-3>.
 - [11] Qimiao Si, Silvio Rabello, Kevin Ingersent, and J. Llewellyn Smith. Locally critical quantum phase transitions in strongly correlated metals. *Nature*, 413(6858):804–808, October 2001. URL <https://doi.org/10.1038/35101507>.
 - [12] T. Senthil, Matthias Vojta, and Subir Sachdev. Weak magnetism and non-Fermi liquids near heavy-fermion critical points. *Phys. Rev. B*, 69(3):035111, January 2004. URL <https://doi.org/10.1103/PhysRevB.69.035111>.
 - [13] Luca de' Medici, Gianluca Giovannetti, and Massimo Capone. Selective Mott Physics as a Key to Iron Superconductors. *Phys. Rev. Lett.*, 112(17):177001, April 2014. URL <https://doi.org/10.1103/PhysRevLett.112.177001>.
 - [14] J. M. Luttinger. Fermi Surface and Some Simple Equilibrium Properties of a System of Interacting Fermions. *Phys. Rev.*, 119(4):1153–1163, August

1960. URL <https://doi.org/10.1103/PhysRev.119.1153>.
- [15] Antoine Georges and Werner Krauth. Physical properties of the half-filled Hubbard model in infinite dimensions. *Phys. Rev. B*, 48(10):7167–7182, September 1993. URL <https://doi.org/10.1103/PhysRevB.48.7167>.
- [16] Goetz Moeller, Qimiao Si, Gabriel Kotliar, Marcelo Rozenberg, and Daniel S. Fisher. Critical Behavior near the Mott Transition in the Hubbard Model. *Phys. Rev. Lett.*, 74(11):2082–2085, March 1995. URL <https://doi.org/10.1103/PhysRevLett.74.2082>.
- [17] Antoine Georges, Gabriel Kotliar, Werner Krauth, and Marcelo J. Rozenberg. Dynamical mean-field theory of strongly correlated fermion systems and the limit of infinite dimensions. *Rev. Mod. Phys.*, 68(1):13–125, January 1996. URL <https://doi.org/10.1103/RevModPhys.68.13>.
- [18] A. Georges, S. Florens, and T. A. Costi. The Mott transition: Unconventional transport, spectral weight transfers, and critical behaviour. *J. Phys. IV Proc.*, 114:165–173, April 2004. URL <http://doi.org/10.1051/jp4:2004114040>.
- [19] Gabriel Kotliar and Dieter Vollhardt. Strongly Correlated Materials: Insights From Dynamical Mean-Field Theory. *Phys. Today*, 57(3):53–59, 2004. URL <https://doi.org/10.1063/1.1712502>.
- [20] N. Mori and T. Watanabe. Pressure effects on the magnetic transition temperatures of NiS₂. *Solid State Commun.*, 27(5):567–569, August 1978. URL [https://doi.org/10.1016/0038-1098\(78\)90396-4](https://doi.org/10.1016/0038-1098(78)90396-4).
- [21] N. Takeshita, S. Takashima, C. Terakura, H. Nishikubo, S. Miyasaka, M. Nohara, Y. Tokura, and H. Takagi. Quantum criticality and disorder in the antiferromagnetic critical point of NiS₂ pyrite, 2007. URL <http://arxiv.org/abs/0704.0591>.
- [22] S. Friedemann, H. Chang, M. B. Gamza, P. Reiss, X. Chen, P. Alireza, W. A. Coniglio, D. Graf, S. Tozer, and F. M. Grosche. Large Fermi Surface of Heavy Electrons at the Border of Mott Insulating State in NiS₂. *Sci. Rep.*, 6(1):25335, July 2016. URL <https://doi.org/10.1038/srep25335>.
- [23] A. Fujimori, I. Hase, H. Namatame, Y. Fujishima, Y. Tokura, H. Eisaki, S. Uchida, K. Takegahara, and F. M. F. de Groot. Evolution of the spectral function in Mott-Hubbard systems with d¹ configuration. *Phys. Rev. Lett.*, 69(12):1796–1799, September 1992. URL <https://doi.org/10.1103/PhysRevLett.69.1796>.
- [24] I. H. Inoue, I. Hase, Y. Aiura, A. Fujimori, Y. Haruyama, T. Maruyama, and Y. Nishihara. Systematic Development of the Spectral Function in the 3d¹ Mott-Hubbard System Ca_{1-x}Sr_xVO₃. *Phys. Rev. Lett.*, 74(13):2539–2542, March 1995. URL <https://doi.org/10.1103/PhysRevLett.74.2539>.
- [25] Bo Gyu Jang, Garam Han, Ina Park, Dongwook Kim, Yoon Young Koh, Yeongkwan Kim, Wonshik Kyung, Hyeong-Do Kim, Cheng-Maw Cheng, Ku-Ding Tsuei, Kyung Dong Lee, Namjung Hur, Ji Hoon Shim, Changyoung Kim, and Gabriel Kotliar. Direct observation of kink evolution due to Hund’s coupling on approach to metal-insulator transition in NiS_{2-x}Se_x. *Nat. Commun.*, 12(1):1208, December 2021. URL <https://doi.org/10.1038/s41467-021-21460-5>.
- [26] H. C. Xu, Y. Zhang, M. Xu, R. Peng, X. P. Shen, V. N. Strocov, M. Shi, M. Kobayashi, T. Schmitt, B. P. Xie, and D. L. Feng. Direct Observation of the Bandwidth Control Mott Transition in the NiS_{2-x}Se_x Multiband System. *Phys. Rev. Lett.*, 112(8), February 2014. URL <https://doi.org/10.1103/PhysRevLett.112.087603>.
- [27] Hiroaki Shishido, Rikio Settai, Hisatomo Harima, and Yoshichika Onuki. A Drastic Change of the Fermi Surface at a Critical Pressure in CeRhIn₅: dHvA Study under Pressure. *J. Phys. Soc. Jpn.*, 74(4):1103–1106, April 2005. URL <https://doi.org/10.1143/JPSJ.74.1103>.
- [28] K. Hashimoto, K. Cho, T. Shibauchi, S. Kasahara, Y. Mizukami, R. Katsumata, Y. Tsuruhara, T. Terashima, H. Ikeda, M. A. Tanatar, H. Kitano, N. Salovich, R. W. Giannetta, P. Walmsley, A. Carrington, R. Prozorov, and Y. Matsuda. A Sharp Peak of the Zero-Temperature Penetration Depth at Optimal Composition in BaFe₂(As_{1-x}P_x)₂. *Science*, 336(6088):1554–1557, June 2012. URL <http://doi.org/10.1126/science.1219821>.
- [29] Xiaoqiang Yao and Jurgen M. Honig. Growth of nickel dichalcogenides crystals with pyrite structure from tellurium melts [NiS₂, NiS_{2-x}Se_x (x ≤ 0.7)]. *Mater. Res. Bull.*, 29(7):709–716, July 1994. URL [https://doi.org/10.1016/0025-5408\(94\)90195-3](https://doi.org/10.1016/0025-5408(94)90195-3).
- [30] J. A. Wilson and G. D. Pitt. Metal-insulator transition in NiS₂. *The Philosophical Magazine: A Journal of Theoretical Experimental and Applied Physics*, 23(186):1297–1310, June 1971. URL <https://doi.org/10.1080/14786437108217003>.
- [31] Yoshiaki Sekine, Hiroki Takahashi, Nobuo Mōri, Takehiko Matsumoto, and Takayuki Kosaka. Effect of pressure on transport properties of Ni(S_{1-x}Se_x)₂. *Physica B: Condensed Matter*, 237–238:148–150, July 1997. URL [https://doi.org/10.1016/S0921-4526\(97\)00078-1](https://doi.org/10.1016/S0921-4526(97)00078-1).
- [32] Craig T. Van Degrift. Tunnel diode oscillator for 0.001 ppm measurements at low temperatures. *Review of Scientific Instruments*, 46(5):599–607, May 1975. URL <http://doi.org/10.1063/1.1134272>.
- [33] K. Götze, M. J. Pearce, M. J. Coak, P. A. Goddard, A. D. Grockowiak, W. A. Coniglio, S. W. Tozer, D. E. Graf, M. B. Maple, P. C. Ho, M. C. Brown, and J. Singleton. Pressure-induced shift of effective ce valence, fermi energy and phase boundaries in CeOs₄Sb₁₂, 2021. URL <https://arxiv.org/abs/2112.03353>.
- [34] D. E. Graf, R. L. Stillwell, K. M. Purcell, and S. W. Tozer. Nonmetallic gasket and miniature plastic turnbuckle diamond anvil cell for pulsed magnetic field studies at cryogenic temperatures. *High Pressure Research*, 31(4):533–543, December 2011. URL <http://doi.org/10.1080/08957959.2011.633909>.
- [35] Supplementary material (to be published).
- [36] T. Shibauchi, A. Carrington, and Y. Matsuda. A Quantum Critical Point Lying Beneath the Superconducting Dome in Iron Pnictides. *Annu. Rev. Condens. Matter Phys.*, 5(1):113–135, March 2014. URL <http://doi.org/10.1146/annurev-conmatphys-031113-133921>.
- [37] Jordan Baglo, Jiasheng Chen, Keiron Murphy, Roos Leenen, Alix McCollam, Michael L. Sutherland, and F. Malte Grosche. Fermi surface and mass renormalization in the iron-based superconductor YFe₂Ge₂, 2021. URL <http://arxiv.org/abs/2104.11791>.
- [38] C. Clark and S. Friedemann. Atomic diffusion in the surface state of Mott insulator NiS₂. *Journal of Magnetism and Magnetic Materials*, 400:56–61, February 2016. URL <https://doi.org/10.1016/j.jmmm.2015.08.012>.
- [39] Shigeki Miyasaka, Hidenori Takagi, Yoshiaki Sekine, Hiroki Takahashi, Nobuo Mōri, and Robert J. Cava. Metal-Insulator Transition and Itinerant Antiferro-

- magnetism in $\text{NiS}_{2-x}\text{Se}_x$ Pyrite. *J. Phys. Soc. Jpn.*, 69(10):3166–3169, October 2000. URL <http://doi.org/10.1143/JPSJ.69.3166>.
- [40] P. G. Niklowitz, M. J. Steiner, G. G. Lonzarich, D. Braithwaite, G. Knebel, J. Flouquet, and J. A. Wilson. Unconventional resistivity at the border of metallic antiferromagnetism in NiS_2 . *Phys. Rev. B*, 77(11), March 2008. URL <http://doi.org/10.1103/PhysRevB.77.115135>.
- [41] Pinaki Majumdar and H. R. Krishnamurthy. Lattice Contraction Driven Insulator-Metal Transition in the $d = \infty$ Local Approximation. *Phys. Rev. Lett.*, 73(11):1525–1528, September 1994. URL <https://doi.org/10.1103/PhysRevLett.73.1525>.
- [42] Yejun Feng, R. Jaramillo, A. Banerjee, J. M. Honig, and T. F. Rosenbaum. Magnetism, structure, and charge correlation at a pressure-induced Mott-Hubbard insulator-metal transition. *Phys. Rev. B*, 83(3), January 2011. URL <https://doi.org/10.1103/PhysRevB.83.035106>.
- [43] S.A. Carter, T.F. Rosenbaum, P. Metcalf, J.M. Honig, and J. Spalek. Mass enhancement and magnetic order at the Mott-Hubbard transition. *Phys. Rev. B*, 48(22):16841–16844, 1993. URL <https://doi.org/10.1103/PhysRevB.48.16841>.
- [44] Alexandru B. Georgescu and Andrew J. Millis. Energy landscape analysis of metal-insulator transitions: theory and application to Ca_2RuO_4 , RNiO_3 and their heterostructures, 2021. URL <http://arxiv.org/abs/2105.02271>.
- [45] Andriy H. Nevidomskyy and P. Coleman. Kondo Resonance Narrowing in d- and f- Electron Systems. *Phys. Rev. Lett.*, 103(14):147205, October 2009. URL <https://doi.org/10.1103/PhysRevLett.103.147205>.
- [46] Antoine Georges, Luca de’Medici, and Jernej Mravlje. Strong Correlations from Hund’s Coupling. *Annu. Rev. Condens. Matter Phys.*, 4(1):137–178, April 2013. URL <http://doi.org/10.1146/annurev-conmatphys-020911-125045>.
- [47] A. Pustogow, R. Rösslhuber, Y. Tan, E. Uykur, A. Böhme, M. Wenzel, Y. Saito, A. Löhle, R. Hübner, A. Kawamoto, J. A. Schlueter, V. Dobrosavljević, and M. Dressel. Low-temperature dielectric anomaly arising from electronic phase separation at the Mott insulator-metal transition. *npj Quantum Mater.*, 6(1): 9, December 2021. URL <https://doi.org/10.1038/s41535-020-00307-0>.
- [48] T.-H. Kim, M. Angst, B. Hu, R. Jin, X.-G. Zhang, J. F. Wendelken, E. W. Plummer, and A.-P. Li. Imaging and manipulation of the competing electronic phases near the Mott metal-insulator transition. *Proceedings of the National Academy of Sciences*, 107(12):5272–5275, March 2010. URL <http://doi.org/10.1073/pnas.1000655107>.
- [49] Fumihiko Nakamura, Mariko Sakaki, Yuya Yamanaoka, Sho Tamaru, Takashi Suzuki, and Yoshiteru Maeno. Electric-field-induced metal maintained by current of the Mott insulator Ca_2RuO_4 . *Sci Rep*, 3(1):2536, December 2013. URL <https://doi.org/10.1038/srep02536>.
- [50] Qiang Han and Andrew Millis. Lattice Energetics and Correlation-Driven Metal-Insulator Transitions: The Case of Ca_2RuO_4 . *Phys. Rev. Lett.*, 121(6): 067601, August 2018. URL <https://doi.org/10.1103/PhysRevLett.121.067601>.
- [51] M. Hartstein, W.H. Toews, Y.-T. Hsu, B. Zeng, X. Chen, M. Ciomaga Hatnean, Q.R. Zhang, S. Nakamura, A.S. Padgett, G. Rodway-Gant, J. Berk, M.K. Kingston, G.H. Zhang, M.K. Chan, S. Yamashita, T. Sakakibara, Y. Takano, J.-H. Park, L. Balicas, N. Harrison, N. Shitsevalova, G. Balakrishnan, G.G. Lonzarich, R.W. Hill, M. Sutherland, and S.E. Sebastian. Fermi surface in the absence of a Fermi liquid in the Kondo insulator SmB_6 . *Nat. Phys.*, 14(2):166–172, 2018. URL <https://doi.org/10.1038/nphys4295>.
- [52] D. Shoenberg. *Magnetic Oscillations in Metals*. Cambridge University Press, Cambridge, 1 edition edition, 1984. ISBN 978-0-521-11878-1. URL <https://doi.org/10.1017/CB09780511897870>.